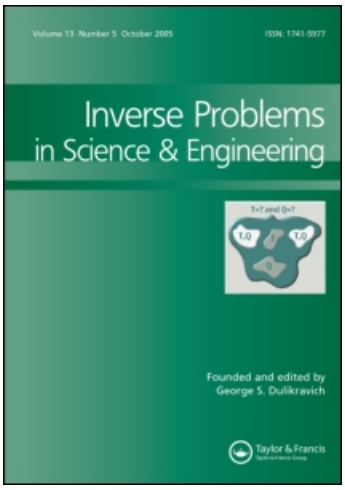

Inverse Problems in Science and Engineering
Publication details, including instructions for authors and subscription information:
http://www.informaworld.com/smpp/title~content=t713643452

Detection of cavities using the method of fundamental solutions

A. Karageorghis [a]; D. Lesnic [b]
[a] Department of Mathematics and Statistics, University of Cyprus, Cyprus [b] Department of Applied Mathematics, University of Leeds, Leeds, UK

First Published:September2009

To cite this Article Karageorghis, A. and Lesnic, D.(2009)'Detection of cavities using the method of fundamental solutions',Inverse Problems in Science and Engineering,17:6,803 — 820
To link to this Article: DOI: 10.1080/17415970802580263
URL: http://dx.doi.org/10.1080/17415970802580263

Inverse Problems in Science and Engineering
Vol. 17, No. 6, September 2009, 803–820

Detection of cavities using the method of fundamental solutions

A. Karageorghis[a]* and D. Lesnic[b]

[a]*Department of Mathematics and Statistics, University of Cyprus, Cyprus;*
[b]*Department of Applied Mathematics, University of Leeds, Leeds, UK*

(*Received 14 January 2008; final version received 3 October 2008*)

The determination of the boundary of a cavity, defined here as a perfectly insulated inclusion, within a conducting medium from a single voltage and current flux measurements on the accessible boundary of the medium, can be modelled as an inverse boundary value problem for harmonic functions. We propose a novel numerical solution method for this inverse problem based on the method of fundamental solutions. The algorithm for imaging the interior of the medium also makes use of radial polar parametrization of the unknown cavity shape in two dimensions (or spherical parametrization in three dimensions). This discretization yields a highly non-linear and ill-conditioned system of equations. The system is recast as a non-linear least-squares problem with penalty regularizing terms included in order to improve the stability of the numerical solution with respect to random noise introduced in the measured error-contaminated input data. The feasibility of this new method is illustrated by some numerical examples.

Keywords: cavity detection; inverse problem; method of fundamental solutions

AMS Subject Classifications: Primary 65N35; Secondary 65N21; 65N38

1. Introduction

It is well known [1] that the mathematical modelling of electrostatic imaging methods in non-destructive testing and evaluation leads to inverse boundary value problems for the Laplace equation. Similarly [2], acoustic imaging leads to inverse boundary value problems for the Helmholtz equation. In these applications, if u denotes the electric potential and $\boldsymbol{n}$ the outward unit normal, given voltage (u) and current flux ($k\partial_n u$) measurements on the accessible boundary $\partial\Omega_2$, we look for an unknown inclusion Ω_1 within a conducting host medium Ω_2 with constant background known conductivity $k > 0$. For simplicity, we consider a doubly-connected two-dimensional annular domain $\Omega = \Omega_2 \backslash \bar{\Omega}_1 \subset \mathbb{R}^2$, with smooth boundary $\partial\Omega$ consisting of two disjoint $\mathcal{C}^2$ curves $\partial\Omega_2$ (exterior boundary) and $\partial\Omega_1$ (interior boundary), such that $\partial\Omega = \partial\Omega_2 \cup \partial\Omega_1$, where $\partial\Omega_2 \cap \partial\Omega_1 = \emptyset$, as shown in Figure 1. In electrostatic imaging methods such as electrical impedance/capacitance tomography, the boundary shape of the interior curve $\partial\Omega_1$ is assessed by imposing a current flux/voltage pattern at a number of electrodes attached to the exterior accessible boundary $\partial\Omega_2$ and

*Corresponding author. Email: andreask@ucy.ac.cy

ISSN 1741–5977 print/ISSN 1741–5985 online

DOI: 10.1080/17415970802580263
http://www.informaworld.com

measuring the resulting voltage/current flux through the electrodes. In thermal imaging, the medium is probed by applying a heat flux/temperature pattern to the boundary $\partial\Omega_2$ and measuring the resulting temperature/heat flux on it.

In principle, we can distinguish three types of boundary conditions on the unknown boundary $\partial\Omega_1$. The determination of a perfectly conducting inclusion Ω_1, which is the case where $k=1$ in Ω, $k=\infty$ in Ω_1, $u=0$ on $\partial\Omega_1$, has been investigated in, for example, [1,3–6]. The determination of a perfectly insulated inclusion Ω_1, i.e. $k=1$ in Ω, $k=0$ in Ω_1, $\partial_n u=0$ on $\partial\Omega_1$, has been investigated in, for example, [4,7,8]. Finally, the determination of an inclusion Ω_1, when $k=1$ in Ω, $0<k<\infty$, $k\neq 1$ in Ω_1, $u_1=u_2$, $\partial_n u_2=k\partial_n u_1$ on $\partial\Omega_1$, called the transmission problem has been investigated in, for example, [9,10]. In the above references we included only studies using boundary integral/element methods, since, in this work, we shall be using a boundary-type approach.

A new inverse algorithm for the determination of a perfectly conducting inclusion has been recently proposed in [11], and it is the goal of the present work to extend this approach to the case of a perfectly insulated inclusion. Numerical examples illustrating the feasibility of the proposed method are provided.

The mathematical formulation of the problem is given in Section 2. The method of fundamental solutions (MFS) and the proposed algorithm are described in Section 3. Numerical results are presented in Section 4 and finally, in Section 5 some conclusions and suggestions for future applications are given.

2. Mathematical formulation

In this section we formulate the direct and inverse problems related to a perfectly insulated inclusion. It is well known from classical potential theory [12,13], that the direct mixed problem given by the Laplace equation

$$\Delta u = 0 \quad \text{in } \Omega, \tag{2.1a}$$

subject to the Dirichlet boundary condition

$$u = f \quad \text{on } \partial\Omega_2, \tag{2.1b}$$

and the homogeneous Neumann boundary condition

$$\partial_n u = 0 \quad \text{on } \partial\Omega_1, \tag{2.1c}$$

has a unique weak solution $u\in\mathcal{H}^1(\Omega)$ if $f\in\mathcal{H}^{1/2}(\partial\Omega_2)$, and a unique classical solution $u\in\mathcal{C}^2(\Omega)\cap\mathcal{C}(\bar{\Omega})$, provided f is sufficiently smooth. This is the case if, for example, $f\in\mathcal{C}^{1+\alpha}(\partial\Omega_2)$, where $\alpha\in(0,1)$. For the definition and properties of the Banach space $\mathcal{C}^{\kappa+\alpha}$, $\alpha\in(0,1)$, $\kappa\in\mathbb{N}$, of $\mathcal{C}^{\kappa}$-functions with derivatives which are Hölder continuous with exponent α, see, for example, [14].

The inverse problem we are concerned with consists of determining not only u but also the perfectly insulated inclusion Ω_1 so that u satisfies the Laplace Equation (2.1a), given the Dirichlet data $f\not\equiv$ constant in (2.1b), the no flux homogeneous Neumann boundary condition (2.1c) and the Neumann current flux measurement

$$g := \partial_n u \quad \text{on } \partial\Omega_2. \tag{2.1d}$$

Clearly, the fact that in the inverse problem the location of Ω_1 is not known is compensated by the additional boundary condition (2.1d). For (2.1a), (2.1c) and (2.1d) to be consistent, we require

$$\int_{\partial\Omega_2} g(s)\mathrm{d}s = 0. \tag{2.2}$$

Compatibility regularity conditions would also require $g \in \mathcal{H}^{-1/2}(\partial\Omega_2)$ for weak solutions, and $g \in \mathcal{C}^{\alpha}(\partial\Omega_2)$ for classical solutions. This type of inverse mathematical model appears in many applications in electric field sensing, see, for example, [15,16].

In contrast to the direct (forward) boundary value problem (2.1a)–(2.1c), the inverse problem (2.1a)–(2.1d) is non-linear and ill-posed.

An important question which is raised concerns uniqueness and, in particular, whether the curve $\partial\Omega_1$ is uniquely determined by the Cauchy data (2.1b) and (2.1d) of a solution u to the boundary value problem (2.1a)–(2.1d).

It can be shown [17], that the identifiability of the curve $\partial\Omega_1$ from a pair of Cauchy data (f, g), $f \not\equiv$ constant, $\int_{\partial\Omega_2} g(s)\mathrm{d}s = 0$, on $\partial\Omega_2$, for the case of a perfectly insulated inclusion satisfying (2.1c) can be reduced to the identifiability of the curve $\partial\Omega_1$ from a pair of Cauchy data (f, g), $f \not\equiv 0$, on $\partial\Omega_2$, for the case of a perfectly conducting inclusion satisfying

$$u = 0, \quad \text{on } \partial\Omega_1, \tag{2.3}$$

and that for the latter inverse problem the solution is unique [1]. Instead of $f \not\equiv$ constant we can require $g \not\equiv 0$.

In [18,19], as well as the derivation of stability estimates, the question of the uniqueness of the solution is addressed. The no-better than logarithmic stability obtained in these articles poses serious limitations to the possibility of finding efficient and robust procedures for reconstructing the inclusion. The response operator

$$F_f(\Omega_1) := \partial_n u|_{\partial\Omega_2} = g, \tag{2.4}$$

defined on a set of admissible subdomains Ω_1 compactly embedded in Ω_2 such that $\Omega = \Omega_2 \backslash \bar{\Omega}_1$ is connected, is a highly non-linear function of the domain Ω_1. Therefore, the extraction of useful information from the measurements (2.1d) is a difficult computational problem. If one is interested only in location search, i.e. sampling whether a given point is inside the cavity or not, then one can employ efficiently the plane or sphere search method for tracking the position of a two- or three-dimensional cavity Ω_1, respectively, as described in [5]. If, on the other hand, the location, shape and size of the obstacle Ω_1 are all of interest, then one can use iterative schemes that require the solution of many forward problems for each change of geometry and position of Ω_1, see [7,8]. These articles use the boundary element method (BEM), or variations of it, as direct solvers. For this type of unknown boundary (free surface), meshless methods such as the MFS are preferred over the BEM. This is primarily due to the fact that in the former, unlike the latter, no elaborate discretization of the boundary is needed and no integral evaluations are involved. This renders the MFS implementation of two- and, especially, three-dimensional problems, much easier than the corresponding BEM implementation. For comprehensive discussions on the merits and drawbacks of the MFS and other meshless methods, the reader is referred to [20–25]. Further, density, convergence and stability MFS analyses are provided in, for example, [26–33].

3. The method of fundamental solutions (MFS)

The MFS has been successfully used in the past for the solution of a variety of free boundary problems. In particular, it has been used for the solution of free boundary problems governed by the Laplace equation [34], the biharmonic equation [35], for axisymmetric free boundary potential problems [36], and for two- and three-dimensional Signorini problems [37,38].

In the application of the MFS to (2.1), we seek an approximation to the solution of Laplace's Equation (2.1a) as a linear combination of fundamental solutions of the form [26,39],

$$u_N(\boldsymbol{c}, \boldsymbol{\xi}; \boldsymbol{x}) = \sum_{k=1}^{2N} c_k \, G(\boldsymbol{\xi}_k, \boldsymbol{x}), \quad \boldsymbol{x} \in \overline{\Omega}, \tag{3.1}$$

where G is the fundamental solution of the two-dimensional Laplace equation, given by

$$G(\boldsymbol{\xi}, \boldsymbol{x}) = -\frac{1}{2\pi} \ln |\boldsymbol{\xi} - \boldsymbol{x}| \, . \tag{3.2}$$

The singularities (sources) $(\boldsymbol{\xi}_k)_{k=\overline{1,2N}}$ are located outside the solution domain Ω, i.e. in $\Omega_1 \cup (\mathbb{R}^2 \backslash \bar{\Omega}_2)$. In particular, $(\boldsymbol{\xi}_k)_{k=\overline{1,N}} \in \Omega_1$ are placed on a (moving) pseudo-boundary $\partial\Omega_1'$ similar to $\partial\Omega_1$, while $(\boldsymbol{\xi}_k)_{k=\overline{N+1,2N}} \in \mathbb{R}^2 \backslash \overline{\Omega}_2$ are placed on a (fixed) pseudo-boundary $\partial\Omega_2'$ similar to $\partial\Omega_2$ as depicted in Figure 1. In the MFS, taking the pseudo-boundary similar to the boundary yields, in general, improved results as has been demonstrated in a recent study by Gorzelańczyk and Kolodziej [40]. In (3.1), the singularities $(\boldsymbol{\xi}_k)_{k=\overline{N+1,2N}}$ are preassigned, whereas the singularities $(\boldsymbol{\xi}_k)_{k=\overline{1,N}}$ move with $\partial\Omega_1$ as will be described in the iterative process presented in the sequel. The fact that the locations of the outer singularities $(\boldsymbol{\xi}_k)_{k=\overline{N+1,2N}}$ are fixed on the artificial pseudo-boundary $\partial\Omega_2'$ means that the latter needs to be dealt with heuristically, see, for example, [41], although Bogomolny [26] suggested that theoretically, the locations of the singularities can be restricted to any surface embracing the given solution domain Ω.

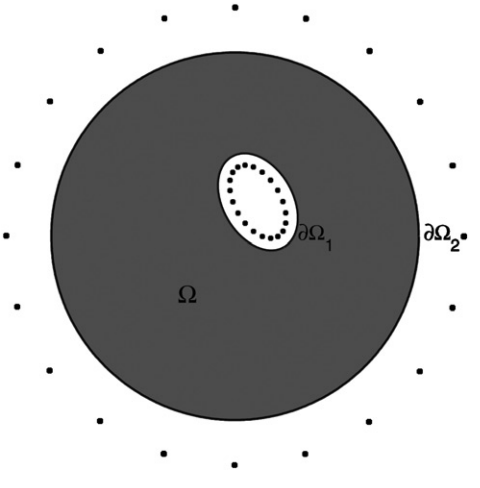

Figure 1. Geometry of the problem. The dots show the location of the singularities in the MFS.

An alternative representation to the MFS representation (3.1) based on the Trefftz series expansion and due to Ramm [42], is

$$u_N(\boldsymbol{a}, \boldsymbol{b}, \boldsymbol{c}, \boldsymbol{d}; \boldsymbol{x}) = a_0 + b_0 \ln(r) + \sum_{k=1}^{N} \left[r^k (a_k \cos(k\vartheta) + b_k \sin(k\vartheta)) + r^{-k} (c_k \cos(k\vartheta) + d_k \sin(k\vartheta)) \right], \tag{3.3}$$

with $\boldsymbol{x} = (r\cos\vartheta,\ r\sin\vartheta)$. Further investigation of this approach is deferred to a future study. Interestingly, a recent article by Chen *et al*. [43] showed some form of equivalence of this approach with the MFS. Further improvements in the application of the MFS to harmonic problems in doubly- and multiply-connected domains are given in [44] and [45], respectively.

Without loss of generality, we shall assume that the (known) fixed exterior boundary $\partial\Omega_2$ is a circle of radius 1 (otherwise one first maps conformally the exterior of Ω_2 onto the exterior of the unit circle). As a result, the outer boundary collocation and source points are chosen as

$$\boldsymbol{x}_{N+\ell} = (\cos\tilde{\vartheta}_\ell,\ \sin\tilde{\vartheta}_\ell), \quad \ell = \overline{1, M}, \tag{3.4}$$

$$\boldsymbol{\xi}_{N+k} = (R\cos\vartheta_k, R\sin\vartheta_k), \quad k = \overline{1, N}, \tag{3.5}$$

respectively, where $\tilde{\vartheta}_\ell = \frac{2\pi(\ell-1)}{M}$, $\ell = \overline{1, M}$ and $\vartheta_k = \frac{2\pi(k-1)}{N}$, $k = \overline{1, N}$ and $R > 1$ is fixed.

Note that we choose $M \geq N$ and therefore in (3.4) we have more (or an equal number of) collocation points than (as) source points in (3.5). We further assume that the unknown boundary $\partial\Omega_1$ is a smooth, star-like curve with respect to the origin. This means that its equation in polar coordinates can be written as

$$x = r(\vartheta)\cos\vartheta,\ y = r(\vartheta)\sin\vartheta, \quad \vartheta \in [0, 2\pi), \tag{3.6}$$

where r is a smooth 2π-periodic function. (A similar but more tedious analysis can be performed in three dimensions through the use of spherical coordinates.)

The insulation condition (2.1c) can therefore be rewritten as

$$0 = \partial_n u|_{r=r(\vartheta)} = -\left[\frac{\partial u}{\partial r} - \frac{1}{r^2} \frac{\partial u}{\partial \vartheta} r'(\vartheta) \right]_{r=r(\vartheta)}. \tag{3.7}$$

Remark that Equation (3.7) requires that the function $r(\vartheta)$ to be differentiable, so, in general, we will seek smooth boundaries $\partial\Omega_1$.

As remarked by Ramm [42], the inverse problems (2.1a), (2.1b), (2.1d), (2.2) and (3.7) may not have a classical solution in the set of star-like domains (3.6). For example, by choosing $f(\vartheta) = \cos(\vartheta)$, $g(\vartheta) = \cos(\vartheta)$, that satisfies (2.2) then $u(r, \vartheta) = r\cos(\vartheta)$ is the unique function satisfying (2.1a), (2.1b) and (2.1d). It cannot, however, satisfy (3.7) which, in this case, becomes

$$0 = -\left[\cos(\vartheta) + \frac{\sin(\vartheta) r'(\vartheta)}{r(\vartheta)} \right], \quad \text{or} \quad r(\vartheta) = \frac{c}{|\sin(\vartheta)|},$$

where c is a constant. As $\vartheta \in [0, 2\pi)$, from this equation it follows that there is no bounded $r(\vartheta)$ that satisfies (3.7). Hence, the inverse problem has no solution.

In each of the numerical examples presented in Section 4 we shall ensure that the inverse problem (2.1a), (2.1b), (2.1d), (2.2) and (3.7) does have a solution.

The discretized form of (3.6) for $\partial\Omega_1$ becomes

$$r_k = r(\vartheta_k), \quad k = \overline{1, N} \tag{3.8}$$

and we choose the inner boundary collocation and source points as

$$\boldsymbol{x}_k = (r_k \cos\vartheta_k, r_k \sin\vartheta_k), \tag{3.9}$$

$$\boldsymbol{\xi}_k = \eta \boldsymbol{x}_k, \quad k = \overline{1, N}. \tag{3.10}$$

The way the parameter $\eta \in (0, 1)$ is chosen is described at the end of this section. An alternative approach proposed in [46,47], and which is based on approximating $r(\vartheta)$ in Fourier series, is not pursued here.

The co-efficients $(c_k)_{k=\overline{1,2N}}$ in (3.1) and the radii $(r_k)_{k=\overline{1,N}} \in (0, 1)$ in (3.8) can be determined by imposing the boundary conditions (2.1b), (2.1c) and (2.1d) in a least-squares sense. This leads to the minimization of the functional

$$\begin{aligned} S(\boldsymbol{c}, \boldsymbol{r}) : = & \sum_{j=N+1}^{N+M} \left[u_N(\boldsymbol{c}, \boldsymbol{\xi}; \boldsymbol{x}_j) - f(x_j)\right]^2 + \sum_{j=N+1}^{N+M} \left[\partial_n u_N(\boldsymbol{c}, \boldsymbol{\xi}; \boldsymbol{x}_j) - g^{\varepsilon}(\boldsymbol{x}_j)\right]^2 \\ & + \sum_{j=1}^{N} \left[\partial_n u_N(\boldsymbol{c}, \boldsymbol{\xi}; \boldsymbol{x}_j)\right]^2 + (\lambda_1 |\boldsymbol{c}|^2)^2 + (\lambda_2 |\boldsymbol{r}|^2)^2, \end{aligned} \tag{3.11}$$

where $\lambda_1, \lambda_2 \geq 0$ are regularization parameters to be prescribed.

Remarks

(i) Equation (3.11) represents a discretized version of the variational form

$$\|u_N - f\|^2_{\mathcal{H}^{1/2}(\partial\Omega_2)} + \|\partial_n u_N - g^{\varepsilon}\|^2_{\mathcal{H}^{-1/2}(\partial\Omega_2)} + \|u_N\|^2_{\mathcal{H}^{1/2}(\partial\Omega_1)},$$

in which, for implementational reasons, all the norms are replaced by the ℓ^2-norm.

(ii) The current flux data (2.1d) comes from practical measurements which are inherently contaminated with noisy errors, and we therefore replace g by g^{ε} such that

$$\|g^{\varepsilon} - g\|_{L^2(\partial\Omega_2)} \leq \varepsilon. \tag{3.12}$$

In computation, the noisy data are generated as

$$g^{\varepsilon}(\boldsymbol{x}_j) = \left(1 + \rho_j p\right) g(\boldsymbol{x}_j), \quad j = \overline{N+1, N+M}, \tag{3.13}$$

where p represents the percentage of noise and ρ_j is a pseudo-random noisy variable drawn from a uniform distribution in $[-1, 1]$ using the NAG [48] routine `G05DAF`.

(iii) In (3.11), the outward normal vector $\boldsymbol{n}$ is defined as follows:

$$\boldsymbol{n} = \begin{cases} \cos\vartheta \boldsymbol{i} + \sin\vartheta \boldsymbol{j}, & \text{if } \boldsymbol{x} \in \partial\Omega_2, \\ \dfrac{1}{\sqrt{r^2(\vartheta) + r'^2(\vartheta)}} [-(r'(\vartheta)\sin\vartheta + r(\vartheta)\cos\vartheta)\boldsymbol{i} + (r'(\vartheta)\cos\vartheta - r(\vartheta)\sin\vartheta)\boldsymbol{j}], & \text{if } \boldsymbol{x} \in \partial\Omega_1, \end{cases} \tag{3.14}$$

where $\boldsymbol{i}=(1,0)$ and $\boldsymbol{j}=(0,1)$. As a result, from (3.1) the normal derivative $\partial_n u_N$ is evaluated as

$$\partial_n u_N = \boldsymbol{n}\cdot\nabla u_N = \sum_{k=1}^{2N} c_k \frac{(\boldsymbol{x}-\boldsymbol{\xi}_k)\cdot\boldsymbol{n}}{|\boldsymbol{x}-\boldsymbol{\xi}_k|^2}. \tag{3.15}$$

In (3.14), we use the finite-difference approximation

$$r'(\vartheta_i) \approx \frac{r_{i+1}-r_{i-1}}{\vartheta_{i+1}-\vartheta_{i-1}}, \quad i=\overline{1,N}, \tag{3.16}$$

with the convention that $r_{N+1}=r_1$, $r_0=r_N$, $\vartheta_{N+1}=0$ and $\vartheta_0=2\pi$.

(iv) Since the inverse problem is ill-posed, in (3.11), the regularization terms $\lambda_1|\boldsymbol{c}|^2$ and $\lambda_2|\boldsymbol{r}|^2$ are added in order to achieve the stability of the numerical solution u and Ω_1.

(v) The constraints $0<r_i<1$, $i=\overline{1,N}$, are imposed during the iterative procedure by adjustment at each iteration.

The minimization of (3.11) is carried out using the MINPACK [49], routine `lmdif` which minimizes the sum of the squares of non-linear functions. In `lmdif`, the Jacobian is calculated internally by forward finite differences. An arbitrary initial guess for the unknowns such as $\boldsymbol{c}=\boldsymbol{c}^{(0)}=0$, $\boldsymbol{r}=\boldsymbol{r}^{(0)}=$constant vector is taken to start the iterative procedure.

In order to determine the optimal value of η in (2.1), we adopt the approach used in [50]. More specifically, the minimization problem is solved for various values of $\eta_\ell=\eta_0+\ell(\delta\eta)$, $\ell=\overline{1,L}$. For each η_ℓ, the maximum error in the boundary conditions at a selected set of uniformly spaced points on the boundary $\partial\Omega$ (different from the boundary collocation points) is calculated. The optimal value of η is chosen as the one for which this maximum error is minimized.

The MFS algorithm described in this section for solving the inverse problem (2.1) in two dimensions can be extended, with obvious modifications, in three dimensions. Note that in three dimensions the fundamental solution of the Laplace equation is $G(\boldsymbol{\xi},\boldsymbol{x})=\frac{1}{4\pi|\boldsymbol{\xi}-\boldsymbol{x}|}$

4. Numerical examples

4.1. *Example 1*

We first consider an example for which an exact solution is known. In particular, we consider

$$\Omega_1=\left\{(x,y)\in\mathbb{R}^2 : x^2+y^2<R_0^2<1\right\}, \quad \Omega_2=\left\{(x,y)\in\mathbb{R}^2 : x^2+y^2<1\right\} \tag{4.1}$$

and

$$u(x,y)=\frac{x}{R_0^2}+\frac{x}{x^2+y^2}. \tag{4.2}$$

For any $0<R_0<1$, the function u satisfies problem (2.1a)–(2.1d), with

$$f(x,y)=x\left(\frac{1}{R_0^2}+1\right) \quad \text{and} \quad g(x,y)=x\left(\frac{1}{R_0^2}-1\right), \quad (x,y)\in\partial\Omega_2. \tag{4.3}$$

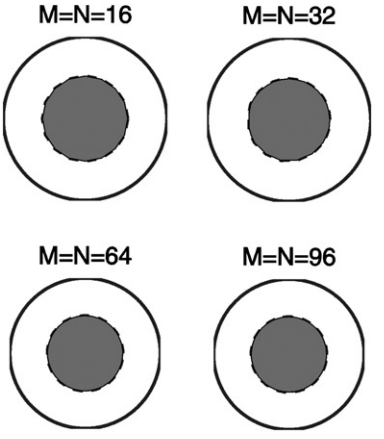

Figure 2. Results for Example 1 with $N = M = 16$, 32, 64 and 96, no noise and $\lambda_1 = \lambda_2 = 0$.

Note that the compatibility condition (2.2) on the Neumann flux data g is automatically satisfied.

In our numerical experiments we consider the case $R_0 = 0.5$.

In Figure 2, we present the approximate solution of the problem for $M = N = 16, 32, 64, 96$, with no noise and with $\lambda_1 = \lambda_2 = 0$. Increasing the value of M over N did not improve the results significantly. We started with an initial guess of a circle of radius equal to $r^{(0)} = 0.3$ and $\boldsymbol{c}^{(0)} = \mathbf{0}$. Experiments were carried out for various values of η defining the distance of the internal pseudo-boundary Ω_1' from the (internal) boundary $\partial\Omega_1$. The exterior circular pseudo-boundary Ω_2' was taken to be the (fixed) circle with radius $R = 2$. As can be observed from these results as $M = N$ increases the approximation tends to the exact solution which is the circle of radius equal to $R_0 = 0.5$. No regularization was found necessary for the test cases investigated in Figure 2 which leads to the conclusion that for no noise, the numerical solution is stable, being unaffected by round-off errors.

Next, we investigate the stability of the recovered inclusion Ω_1 with respect to $p = 1\%$ noisy perturbations in the Neumann data g introduced in (3.13). In order to assess the accuracy of the numerical solution we calculated the maximum error in the final positions of the points defining the cavity, namely,

$$E_r = \max_{1 \le k \le N} |r_k - R_0|.$$

Clearly, the smaller the E_r, the better the solution. In Figure 3 we present the plot of E_r versus the regularization parameters $\lambda_1 = \lambda_2$ for $N = M = 32$, 64 and 96. From these plots, it appears that the best results are obtained, in all cases, for $\lambda_1 = \lambda_2 = 10^{-3}$. The shape of the resulting cavities for some values of $\lambda_1 = \lambda_2$ are presented in Figures 4–6, for $N = M = 32$, 64 and 96, respectively, confirming the predictions of Figure 3.

In Figure 7, we present the plots of E_r versus λ_1 when $\lambda_2 = 0$ and E_r versus λ_2 when $\lambda_1 = 0$, for $N = M = 64$, with noise $p = 1\%$. When $\lambda_2 = 0$, the regularization parameter λ_1 improves the accuracy leading to a minimum for E_r at $\lambda_1 = 10^{-3}$. A similar, but not as pronounced, behaviour is observed when $\lambda_1 = 0$ and λ_2 is varied. In this case, the improvement when the regularization parameter $\lambda_2 = 10^{-3}$ is not as marked as in the corresponding case for $\lambda_2 = 0$. These observations are confirmed by Figures 8 and 9, where

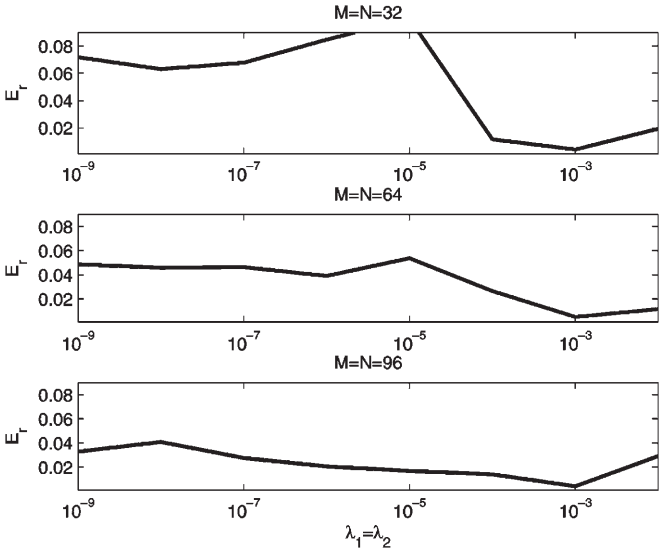

Figure 3. E_r versus $\lambda_1 = \lambda_2$ for $N = M = 32$, 64 and 96, noise $p = 1\%$ in Example 1.

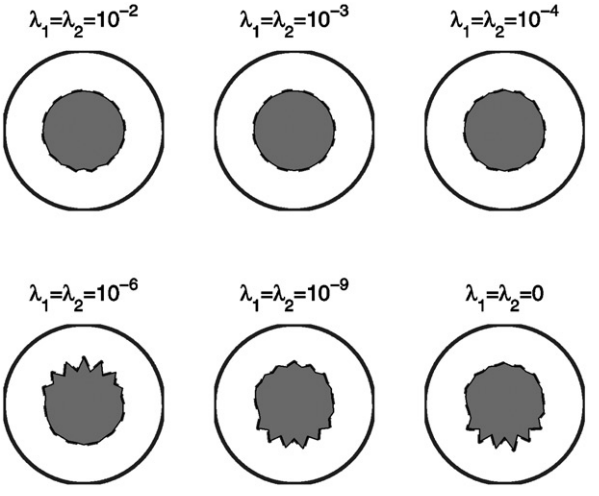

Figure 4. Results for Example 1 with $N = M = 32$, noise $p = 1\%$ for various values of $\lambda_1 = \lambda_2$.

the shapes of the corresponding cavities are presented, for selected values of λ_1 and λ_2. Overall, from Figures 5, 8 and 9 it can be seen that regularization is necessary in both λ_1 and $\lambda_2 > 0$ in order to achieve an accurate and stable Ω_1 reconstruction which is comparable with the percentage of noise p introduced in the input measured data (3.13). The choice of the regularization parameters λ_1 and λ_2 was based on trial and error. More rigorous choices such as the L-surface method [51] could be investigated in future work.

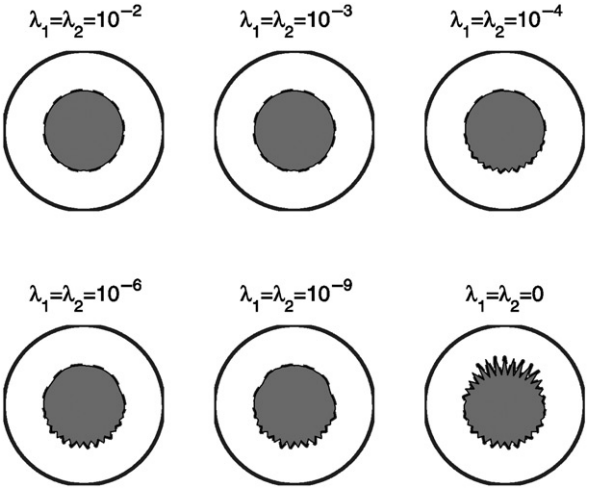

Figure 5. Results for Example 1 with $N = M = 64$, noise $p = 1\%$ for various values of $\lambda_1 = \lambda_2$.

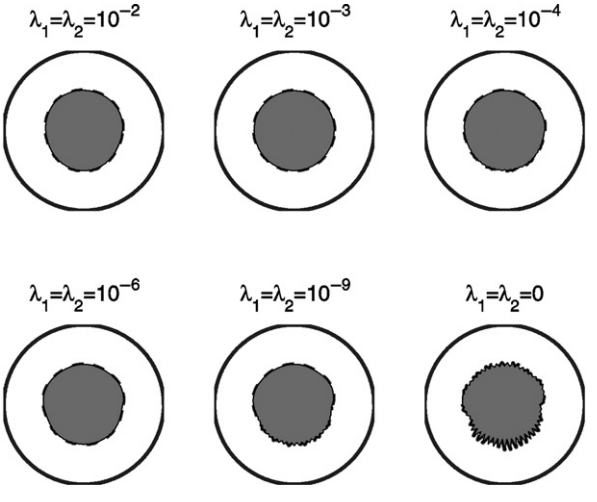

Figure 6. Results for Example 1 with $N = M = 96$, noise $p = 1\%$ for various values of $\lambda_1 = \lambda_2$.

4.2. *Example 2*

In this example, we consider the more complicated peanut-shaped cavity $\partial\Omega_1$ given by the radial parametrization

$$r(\vartheta) = \frac{3}{4}\sqrt{\cos^2(\vartheta) + 0.25\sin^2(\vartheta)}, \quad \vartheta \in [0, 2\pi). \tag{4.4}$$

The Dirichlet data (2.1b) on $\partial\Omega_2$ is taken as [8]

$$u(1, \vartheta) = f(\vartheta) = \mathrm{e}^{-\cos^2\vartheta}, \quad \vartheta \in [0, 2\pi). \tag{4.5}$$

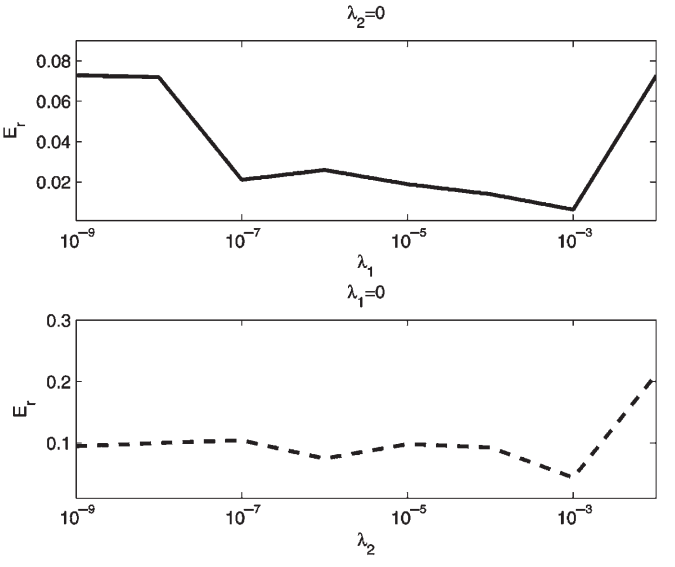

Figure 7. E_r versus λ_1 when $\lambda_2 = 0$ and E_r versus λ_2 when $\lambda_1 = 0$, for $N = M = 64$, noise $p = 1\%$ in Example 1.

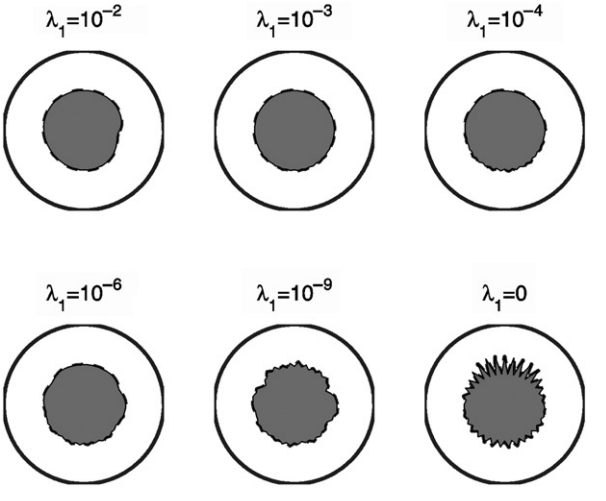

Figure 8. Results for Example 1 with $N = M = 64$, noise $p = 1\%$ for various values of λ_1 when $\lambda_2 = 0$.

Since in this case no analytical solution is available, the Neumann data (2.1d) is simulated by solving the direct mixed well-posed problem (2.1a), (2.1c) and (4.5), when $\partial\Omega_1$ is given by (4.4), using the MFS with $M = N = 96$. In order to avoid committing an inverse crime, the inverse solver is applied using a different number $M = N = 64$. Furthermore, noise is added as in (3.13). The initial guess was taken to be a circle of radius $r^{(0)} = 0.5$ and $\boldsymbol{c}^{(0)} = \mathbf{0}$. In Figure 10 we present the reconstructed and the exact shapes obtained with no

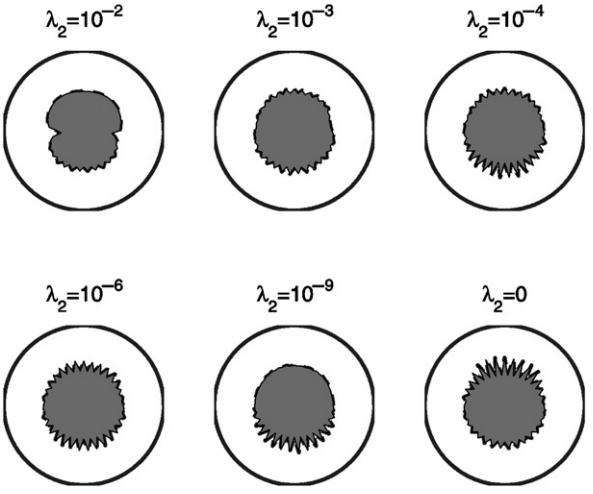

Figure 9. Results for Example 1 with $N = M = 64$, noise $p = 1\%$ for various values of λ_2 when $\lambda_1 = 0$.

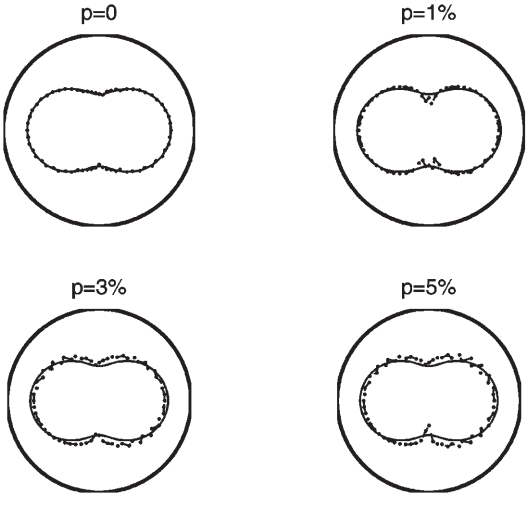

Figure 10. Results with no regularization for Example 2 with $N = M = 64$, for noise $p = 0$, 1%, 3% and 5%.

regularization, when the percentage of noise is $p = 0, 1\%, 3\%$ and 5%. From this figure it can be seen that the reconstructed shape is in excellent agreement with the shape of the cavity we seek when no noise is present, i.e. when $p = 0$. As expected, the reconstructed shape gradually deteriorates as the noise level increases. In Figures 11–13, we present the reconstructed and the exact shapes obtained with regularization, for noise levels $p = 1\%$, 3% and 5%, respectively. From these figures it can be seen that there is an indication that the optimal improvements of regularization are obtained for $\lambda_1 = \lambda_2 = 10^{-6}$.

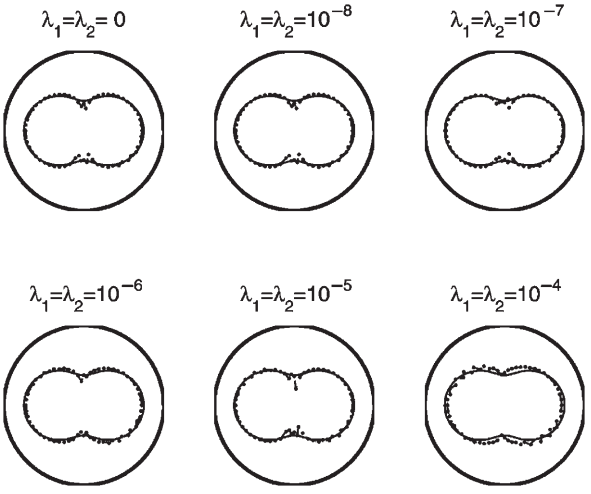

Figure 11. Effect of regularization in Example 2 with $N = M = 64$, with noise $p = 1\%$.

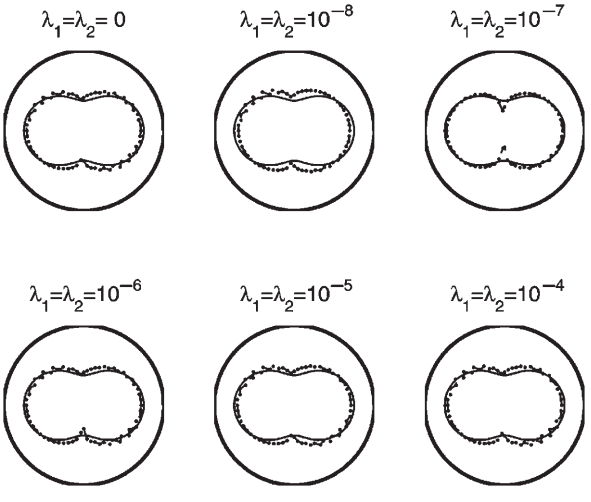

Figure 12. Effect of regularization in Example 2 with $N = M = 64$, with noise $p = 3\%$.

4.3. *Example 3*

Finally, we consider a bean-shaped obstacle Ω_1 given by the radial parametrization

$$r(\vartheta) = \frac{0.5 + 0.4\cos(\vartheta) + 0.1\sin(2\vartheta)}{1 + 0.7\cos(\vartheta)}, \quad \vartheta \in [0, 2\pi). \tag{4.6}$$

This example, which was also considered in [8], is more difficult than Example 2 because of the presence of a sharp cusp-like portion mimicking a re-entrant corner. The same Dirichlet data (4.5) was taken and all the numerical details are the same as in Example 2. In Figure 14 we present the reconstructed and the exact shapes obtained with no

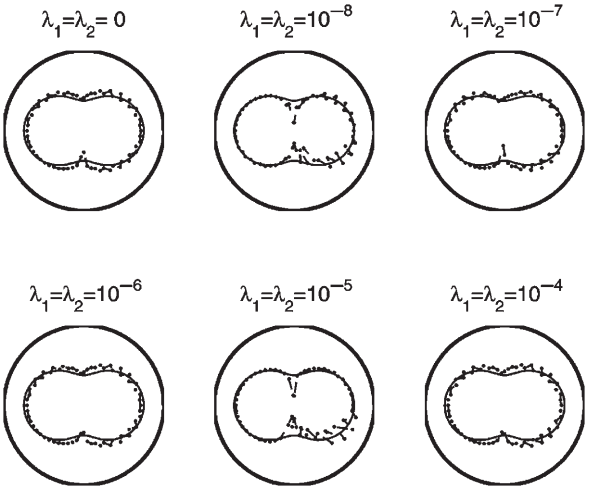

Figure 13. Effect of regularization in Example 2 with $N = M = 64$, with noise $p = 5\%$.

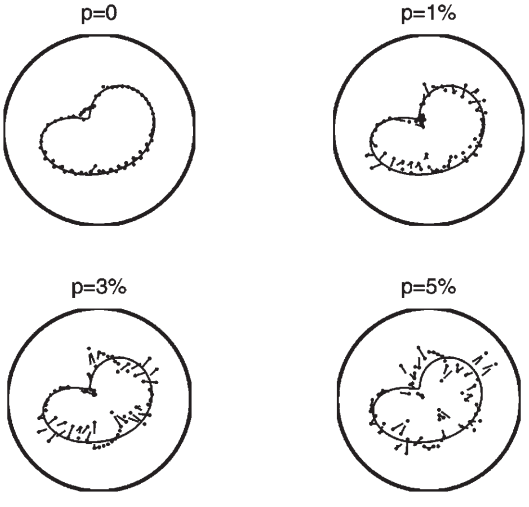

Figure 14. Results with no regularization for Example 3 with $N = M = 64$, for noise $p = 0$, 1%, 3% and 5%.

regularization, when the percentage of noise is $p = 0$, 1%, 3% and 5%. As in the case of Example 2, when no noise is present, the reconstructed shape is in good agreement with the shape of the cavity defined by (4.6). However, as the noise level is increased, the reconstructed shape deteriorates and becomes unstable. These instabilities can be alleviated using positive regularization parameters in (3.11) as was done with the simpler Examples 1 and 2. Alternatively, according to the discrepancy principle [52], regularization may be achieved by imposing fewer function evaluations in the non-linear minimization routine `lmdif` at a level at which the objective functional (3.11) with $\lambda_1 = \lambda_2 = 0$ becomes comparable with ε^2, where ε is given by (3.12). The results obtained using this procedure,

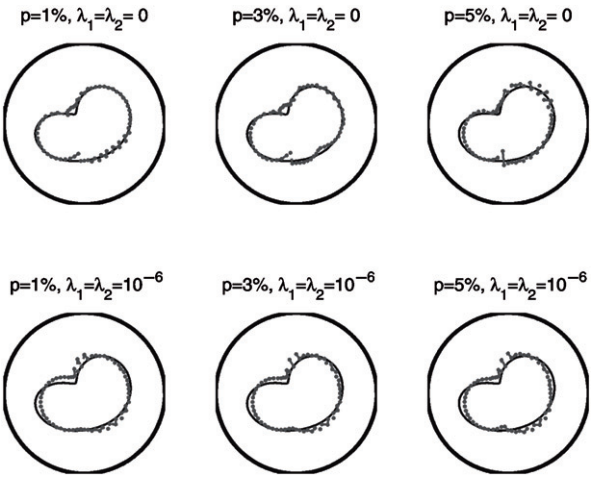

Figure 15. Results with and without regularization and fewer function evaluations for Example 3 with $N = M = 64$, and noise $p = 1\%$, 3% and 5%.

i.e. fewer function evaluations, are presented in the the top row of Figure 15. In comparison with the results presented in Figure 14, it can be seen that smoother and stable cavities are retrieved. Moreover, the inclusion of non-zero regularization parameters λ_1 and λ_2 in (3.11) in conjunction with imposing a smaller number of function evaluations in `lmdif` produce slightly improved results which are presented in the bottom row of Figure 15. These results also agree qualitatively with the numerical results presented in [8], obtained using a BEM.

5. Conclusions

A novel numerical method based on a regularized iterative MFS has been developed for the approximate solution of an inverse (insulated) cavity problem. The MFS was employed because while it shares most of the advantages of the BEM for such free boundary-type problems, it is considerably easier to implement and does not involve potentially troublesome integrations. The method employed involved choosing several parameters such as the numbers of degrees of freedom N and M, the fraction η dictating the distance between the sought cavity $\partial\Omega_1$ and its corresponding pseudo-boundary $\partial\Omega_1'$, the regularization parameters λ_1 and λ_2, and the number of function evaluations imposed in the non-linear minimization routine `lmdif`. The selection of these parameters has been the subject of extensive experimentation. The method was applied to three such problems and the effect of regularization was studied for noisy data up to 5%. The numerical results indicate that accurate reconstructions with reasonable stability against noisy data can be produced with the proposed method. Further numerical experiments indicated that for a noise level above 10% the reconstructions began to deteriorate significantly. Possible areas of future research related to the technique presented in this study are: (i) The extension of the technique to the detection of multiple cavities within a conducting medium, (ii) the application to acoustic cavity imaging and (iii) the computational extension of the algorithm to three-dimensional problems.

Acknowledgements

The authors would like to thank the UK Royal Society and the University of Cyprus for supporting this research.

References

[1] R. Kress, *Inverse Dirichlet problem and conformal mapping*, Math. Comput. Simulation 66 (2004), pp. 255–265.
[2] K. Erhard and R. Potthast, *The point source method for reconstructing an inclusion from boundary measurements in electrical impedence tomography and acoustic scattering*, Inverse Probl. 19 (2003), pp. 1139–1157.
[3] R. Chapko and R. Kress, *A hybrid method for inverse boundary value problems in potential theory*, J. Inverse Ill-Posed Probl. 13 (2005), pp. 27–40.
[4] E. Divo, A.J. Kassab, and F. Rodriguez, *An efficient singular superposition technique for cavity detection and shape optimization*, Numer. Heat Transfer, Part B: Fundamentals 46 (2004), pp. 1–30.
[5] S. Kim, O. Kwon, and J.K. Seo, *Location search techniques for a grounded conductor*, SIAM J. Appl. Math. 62 (2002), pp. 1383–1393.
[6] R. Kress and W. Rundell, *Nonlinear integral equations and the iterative solution for an inverse boundary value problem*, Inverse Prob. 21 (2005), pp. 1207–1223.
[7] R. Duraiswami, G.L. Chahine, and K. Sarkar, *Boundary element techniques for efficient 2-D and 3-D electrical impedance tomography*, Chem. Eng. Sci. 52 (1997), pp. 2185–2196.
[8] O. Ivanyshyn and R. Kress, *Nonlinear integral equations for solving inverse boundary value problems for inclusions and cracks*, J. Integral Eqns. Appl. 18 (2006), pp. 13–38.
[9] T. Murai and Y. Kagawa, *Boundary element iterative techniques for determining the interface boundary between two Laplace domains – A basic study of impedance plethysmography as an inverse problem*, Internat. J. Numer. Methods Eng. 23 (1986), pp. 35–47.
[10] J.C. de Munck, T.J.C. Faes, and R.M. Heethaar, *The boundary element method in the forward and inverse problem of electrical impedance tomography*, IEEE Trans. Biomed. Eng. 47 (2000), pp. 792–800.
[11] D. Borman, D.B. Ingham, B.T. Johansson, and D. Lesnic, *The method of fundamental solutions for the detection of cavities in EIT*, J. Integral Eqns. Appl. (accepted).
[12] R. González and R. Kress, *On the treatment of a Dirichlet–Neumann mixed boundary value problem for harmonic functions by an integral equation method*, SIAM J. Math. Anal. 8 (1977), pp. 504–517.
[13] W. McLean, *Strongly Elliptic Systems and Boundary Integral Equations*, Cambridge University Press, Cambridge, 2000.
[14] O.A. Ladyzenskaya, V.A. Solonnikov, and N.N. Uraltserva, *Linear and Quasilinear Equations of Parabolic Type*, Transactions of the Mathematical Monographs, Vol. 23, AMS, Providence, RI, 1968.
[15] J.R. Smith, *Field mice: extracting hand geometry from electric field measurements*, IBM Sys. J. 35 (1996), pp. 587–608.
[16] J.R. Smith, T. White, C. Dodge, J. Paradiso, N. Gershenfeld, and D. Allport, *Electric field sensing for graphical interfaces*, IEEE Comput. Graphics Appl. 18 (1998), pp. 54–60.
[17] H. Haddar and R. Kress, *Conformal mappings and inverse boundary value problems*, Inverse Probl. 21 (2005), pp. 935–953.
[18] G. Alessandrini and L. Rondi, *Optimal stability for the inverse problem of multiple cavities*, J. Diff. Eq. 176 (2001), pp. 356–386.
[19] G. Alessandrini, A. Morassi, and E. Rosset, *Detecting cavities by electrostatic boundary measurements*, Inverse Probl. 18 (2002), pp. 1333–1353.

[20] G. Fairweather and A. Karageorghis, *The method of fundamental solutions for elliptic boundary value problems*, Adv. Comput. Math. 9 (1998), pp. 69–95.
[21] M.A. Golberg and C.S. Chen, *Discrete Projection Methods for Integral Equations*, Computational Mechanics Publications, Southampton, 1997.
[22] M.A. Golberg and C.S. Chen, *The method of fundamental solutions for potential, Helmholtz and diffusion problems*, *Boundary Integral Methods: Numerical and Mathematical Aspects, vol. 1 of Comput. Eng*, WIT Press/Computational Mechanics Publication, Boston, MA, 1999, pp. 103–176.
[23] U. Heise, *Numerical properties of integral equations in which the given boundary values and the sought solutions are defined on different curves*, Comput. Struct. 8 (1978), pp. 199–205.
[24] G. de Mey, *Integral equations for potential problems with the source function not located on the boundary*, Comput. Struct. 8 (1978), pp. 113–115.
[25] G. Burgess and E. Maharejin, *A comparison of the boundary element and superposition methods*, Comput. Struct. 19 (1984), pp. 697–705.
[26] A. Bogomolny, *Fundamental solutions method for elliptic boundary value problems*, SIAM J. Numer. Anal. 22 (1985), pp. 644–669.
[27] M. Katsurada and H. Okamoto, *The collocation points of the fundamental solution method for the potential problem*, Comput. Math. Appl. 31 (1996), pp. 123–137.
[28] T. Kitagawa, *Asymptotic stability of the fundamental solution method*, J. Comput. Appl. Math. 38 (1991), pp. 263–269.
[29] V.D. Kupradze and M.R. Aleksidze, *The method of functional equations for the approximate solution of certain boundary value problems*, USSR Comput. Maths. Math. Phys. 4 (1964), pp. 82–126.
[30] X. Li, *On the convergence of the method of fundamental solutions for solving the Dirichlet problem of Poisson equation*, Adv. Comput. Math. 23 (2005), pp. 265–277.
[31] P. Mitic and Y.F. Rashed, *Convergence and stability of the method of meshless fundamental solutions using an array of randomly distributed sources*, Eng. Anal. Boundary Elem. 28 (2004), pp. 143–153.
[32] Y.-S. Smyrlis and A. Karageorghis, *Some aspects of the method of fundamental solutions for certain harmonic problems*, J. Sci. Comput. 16 (2001), pp. 341–371.
[33] Th. Tsangaris, Y.-S. Smyrlis, and A. Karageorghis, *Numerical analysis of the method of fundamental solutions for harmonic problems in annular domains*, Numer. Methods Partial Diff. Eq. 22 (2006), pp. 507–539.
[34] A. Karageorghis, *The method of fundamental solutions for the solution of steady-state free boundary problems*, J. Comput. Phys. 98 (1992), pp. 119–128.
[35] A. Poullikkas, A. Karageorghis, G. Georgiou, and J. Ascough, *The method of fundamental solutions for Stokes flows with a free surface*, Numer. Methods Partial Diff. Eq. 14 (1998), pp. 667–678.
[36] A. Karageorghis and G. Fairweather, *The method of fundamental solutions for axisymmetric potential problems*, Internat. J. Numer. Methods Eng. 44 (1999), pp. 1653–1669.
[37] A. Poullikkas, A. Karageorghis, and G. Georgiou, *The method of fundamental solutions for Signorini problems*, IMA J. Numer. Anal. 18 (1998), pp. 273–286.
[38] A. Poullikkas, A. Karageorghis, and G. Georgiou, *The numerical solution of three dimensional Signorini problems with the method of fundamental solutions*, Eng. Anal. Boundary Elem. 25 (2001), pp. 221–227.
[39] R. Mathon and R.L. Johnston, *The approximate solution of elliptic boundary-value problems by fundamental solutions*, SIAM J. Numer. Anal. 14 (1977), pp. 638–650.
[40] P. Gorzelańczyk and J.A. Kołodziej, *Some remarks concerning the shape of the source contour with application of the method of fundamental solutions to elastic torsion of prismatic rods*, Eng. Anal. Boundary Elem. 32 (2008), pp. 64–75.
[41] K. Balakrishnan and P.A. Ramachandran, *The method of fundamental solutions for linear diffusion-reaction equations*, Math. Comput. Model. 31 (2000), pp. 221–237.

[42] A.G. Ramm, *A geometrical inverse problem*, Inverse Probl. 2 (1986), pp. L19–L21.
[43] J.T. Chen, C.S. Wu, Y.T. Lee, and K.H. Chen, *On the equivalence of the Trefftz method and method of fundamental solutions for Laplace and biharmonic equations*, Comput. Math. Appl. 53 (2007), pp. 851–879.
[44] D.L. Young, K.H. Chen, and C.W. Lee, *Novel meshless method for solving the potential problems with arbitrary domain*, J. Comput. Phys. 209 (2005), pp. 290–321.
[45] K.H. Chen, J.H. Kao, J.T. Chen, D.L. Young, and M.C. Lu, *Regularized meshless method for multiply-connected-domain Laplace problems*, Eng. Anal. Boundary Elem. 30 (2006), pp. 882–896.
[46] C.J.S. Alves and N.F.M. Martins, *The method of fundamental solutions applied to a heat conduction inverse problem*, in *III European Conference on Computational Mechanics, Solids, Structures and Coupled Problems in Engineering*, C.A. Mota Soares et al., eds., Lisbon, Portugal, 2006, 5–8 June.
[47] Y.Z. Ider, B. Nakiboglu, M. Kuzuoglu, and N.G. Gençer, *Determination of the boundary of an object inserted into a water-filled cylinder*, Clin. Phys. Physiol. Meas. 13 (1992), pp. 151–154.
[48] Numerical Algorithms Group Library Mark 21, NAG(UK) Ltd, Wilkinson House, Jordan Hill Road, Oxford, UK, 2007.
[49] B.S. Garbow, K.E. Hillstrom, and J.J. Moré, *MINPACK Project*, Argonne National Laboratory, Argonne, Illinois, 1980.
[50] R. Tankelevich, G. Fairweather, A. Karageorghis, and Y.-S. Smyrlis, *Potential field based geometric modelling using the method of fundamental solutions*, Internat. J. Numer. Methods Eng. 68 (2006), pp. 1257–1280.
[51] M. Belge, M.E. Kilmer, and E.L. Miller, *Efficient determination of multiple regularization parameters in a generalized L-curve framework*, Inverse Probl. 18 (2002), pp. 1161–1183.
[52] A. Morozov, *On the solution of functional equations by the method of regularization*, Soviet Math. Dokl. 7 (1966), pp. 414–417.